RSC Advances

ROYAL SOCIETY OF CHEMISTRY

www.rsc.org/advances

Fabrication of $CuO\text{-}1.5ZrO_2$ composite thin film, from heteronuclear molecular complex and its electrocatalytic activity towards methanol oxidation

Muhammad Ali Ehsan,[a] *Abbas Saeed Hakeem,*[a] *Hamid Khaledi,*[b] *Muhammad Mazhar,*[b]* *Muhammad Mehmood Shahid,*[c] *Alagarsamy Pandikumar,*[c] and *Nay Ming Huang* [c]

[*a*] Center of Research Excellence in Nanotechnology (CENT), King Fahd University of Petrolium & Minerals, Saudia Arabia.

[*b*]*Department of Chemistry, Faculty of Science, University of Malaya, Lembah Pantai, 50603-Kuala Lumpur, Malaysia.

[*c*] Department of Physics, Faculty of Science, University of Malaya, Lembah Pantai, 50603-Kuala Lumpur, Malaysia.

**Corresponding author's e-mail*: mazhar42pk@yahoo.com, Tel.: +60379674269;

Fax: +60379674193

Keywors: Molecular precursor; $CuO\text{-}1.5ZrO_2$ composite; Thin films; Electro-catalytic activity; AACVD.

Abstract

A heteronuclear coordination complex $[Cu_4Zr_6(\mu\text{-}O)_8(dmap)_4(OAc)_{12}]\bullet H_2O$ (**1**), where dmap = *N,N*-dimethylaminopropanolato and ^-OAc = acetato, has been isolated in pure form by the chemical interaction of $Zr(dmap)_4$ with $Cu(OAc)_2\cdot H_2O$ in THF. Complex (**1**) has been examined by melting point, elemental analysis, FT-IR spectroscopy and single crystal X-ray diffraction.

The thermal decomposition behavior of the complex has been explored by thermogravimetric, derivative thermogravimetric and differential scanning calorimetric analyses which reveal that complete conversion of (**1**) into 1:1.5 composite oxides, CuO: ZrO_2, treated at 500 ˚C. The ability of complex (**1**) to act as a single-source precursor for the formation of advanced composite oxides thin film has been investigated by aerosol assisted chemical vapor deposition at 550 ˚C in air ambient. Scanning electron microscopy (SEM), energy dispersive X-ray (EDX), X-ray powder diffraction (XRD) and X-ray photoelectron spectroscopic (XPS) analyses of the developed thin films suggest the formation of good quality crystalline microspherical-shaped CuO-1.5ZrO_2 composite oxide with high purity. The electrocatalytic activity of CuO-1.5ZrO_2 composite oxide film was studied toward methanol oxidation in an alkaline medium and it showed high oxidation peak current of 14 μA during a forward scan which is ~3.5-fold higher than the bare Pt electrode. The ease and low cost fabrication and high electrocatalytic activity of composite oxide film could make it potential candidate for direct methanol fuel cells application.

1. Introduction

Heteronuclear complexes are of interest not only because of their attractive structural chemistry, [1] catalytic properties [2] and potential for industrial applications [2] but also because they constitute a group of molecular precursors for creating advanced ceramic materials.[3] The high applicability of such compounds is an outcome of the cooperation between two different metals in a single molecule which give rise to properties that are not a simple sum of the properties of the individual metals and are often crucial for a system to achieve the desired activity. Heteronuclear compounds containing suitable chelating groups are regarded as single source molecular precursors (SSMPs) and are highly appreciated because of the ease of synthesis, lower energetic demand, less complicated product mixtures and the potential to tune the materials' outcome by

adjusting the molecular stoichiometry and structure.[4, 5] These molecular precursor complexes frequently display other attractive features including high solubility in common organic solvents, increased hydrolytic stability, ease of purification, and in some cases volatility.[6, 7] This combination of physical and chemical properties generally allows SSMPs to be used in sol-gel, metal-organic chemical vapor deposition or metal-organic decomposition processes for the preparation of pure advanced bi- or multimetallic oxide materials with high crystallinity and desirable morphologies at relatively lower temperatures or shorter calcination periods.[8, 9] However, to meet such potential advantages, the molecular precursor must involve bridging moieties which contribute to their volatility and clean controlled thermal decomposition without incorporating side reactions or by-products. For this purpose, we have examined the abilities of acetate, *β*-diketonate and aminoalkoxide ligands to associate two different metal centers in a specific ratio within a heteronuclear system.[10-15] The utilization of these heteronuclear precursors in an aerosol assisted chemical vapor deposition (AACVD) has become a well-established route for the fabrication of advanced metal oxide films.

A survey of known heterobimetallic Cu-Zr complexes includes a series of compounds, [(RCOCHCOR')Cu{Zr_2(OPr-i)}] (R = R' =Me (1); R = R' = CF_3 (2) and R = Me, R' = CF_3 (3)), which have been spectroscopically probed.[16] Some interesting zirconium copper(I) [$Zr_4Cu_4(\mu_4$-O)(μ-$OPr^i)_{10}(OPr^i)_8$][17] and zirconium copper(II) oxo-isopropoxo [$Zr_4Cu_4(\mu_4$-$O)_3$(μ-$OPr^i)_{10}(OPr^i)_8$][18] complexes have also been structurally characterized. However, the thermal degradation pathways of these Cu-Zr complexes and their potential as CVD precursor for the synthesis of composite oxides nanopowders or thin films have not been investigated so far.

Previously we designed and synthesized a well-defined heterobimetallic complex [$Cu_4Zr_2(\mu_4$-$O)_2$(dmae)$_4$(OAc)$_8$]•2H_2O using *N,N*-dimethylaminoethanolato (dmae) as bridging moiety

between two metal centers and the thermal decomposition of this complex resulted in formation of $CuZrO_3$-CuO thin films.[19] The continuation of similar synthetic strategy enabled us to construct a new Cu-Zr heterometallic derivative complex $[Cu_4Zr_6(\mu\text{-}O)_8(dmap)_4(OAc)_{12}]\bullet H_2O$ through a different aminoalcoholic bridging moiety, 3-dimethylamino-1-propanolato $(CH_3)_2N(CH_2)_3O^-$; dmap), which exhibits different stoichiometry as compare to the earlier reported complex.[19] A new bridging connectivity pattern has been achieved within the heterometallic assembly to produce a novel and modified heterometallic complex with improved physicochemical properties. The complex (**1**) decomposes under ordinary aerosol assisted chemical vapor deposition (AACVD) conditions to yield impurity free target material (CuO-$1.5ZrO_2$) inspite of increasing number of carbons in damp ligand. Further, the CuO-$1.5ZrO_2$ thin film electrodes of high temperature material have been fabricated at relatively low temperature which is another unique prospective achieved through complex (**1**).

Considering future commercial-scale availability from coal gasification and natural gas modification, high sensitivity to catalysts and easy conversion to chemicals, methanol has gained importance as an important feedstock for chemical industry, especially in fuel cells.[20] In an electrochemical oxidation of methanol, the electrode material is an important parameter where high efficiency electrocatalyst is needed. Zirconia based copper oxide nanocomposites have been shown to perform numerous catalytic operations such as methanol synthesis, [21, 22] water gas shift reactions, [23, 24] NO and N_2O decompositions[25] and various hydrogenation reactions.[26, 27] The high catalyst activity is mainly accounted by the presence of zirconia which presents special characteristics such as high fracture toughness, ionic conductivity and stability even under reducing conditions.[28] Moreover, the possession of both amphoteric and redox functions, rich surface oxygen vacancies[29] and surface hydroxyl groups[30,31] make it superior when compared

with conventional copper oxide-zinc oxide catalyst for numerous catalytic applications. Recent literature reveals many ways of producing binary CuO-ZrO_2 nanopowders including deposition-precipitation,[23] precipitation,[32] surfactant assisted method[26] and sol-gel method.[33] However, the fabrication of copper oxide-zirconia composite thin film electrodes is not frequently addressed in the literature.

In the present work, we aim to report the synthesis, structural characterization and thermal characteristics of a new heterobimetallic complex $[Cu_4Zr_6(\mu\text{-}O)_8(dmap)_4(OAc)_{12}]\bullet H_2O$ (**1**), (dmap = *N,N*-dimethylaminopropanolate; $^-$OAc = acetato) for the single step growth of CuO-1.5ZrO_2 composite oxide thin film electrodes on fluorine doped tin oxide coated (FTO) conducting glass substrate at 550 °C via AACVD technique. The deposited electrodes were characterized by XRD, SEM, EDX and XPS for their phase, structural, textural and compositional recognition. The electrocatalytic activity of CuO-1.5ZrO_2 composite oxide electrodes was studied toward methanol oxidation in an alkaline medium and it showed high oxidation peak current of 14 μA during a forward scan which is ~3.5-fold higher than the bare Pt electrode. Considering the high cost of Pt, the present metal oxide composite catalyst is potential alternative for direct methanol fuel cells towards methanol oxidation.

2. Experimental

2.1. General consideration

All synthetic reactions were carried out using standard Schlenk technique fitted with vacuum line and hot plate arrangements under an atmosphere of purified argon. THF solvent was purified by refluxing over sodium benzophenoate for several hours and distilled immediately prior to use. Copper (II) acetate dihydrate, zirconium (IV) isopropoxide and *N*-*N*-dimethylamino-1-propanol (dmapH) (Aldrich Chemical Co.) $Zr(dmap)_4$ was prepared by literature procedures.[34, 35] The

elemental analyses were performed using Leco CHNS 932. Infrared spectrum was collected on a single reflectance ATR instrument (4000–400 cm^{-1}, resolution 4 cm^{-1}). Thermal analyses were performed on a Perkin Elmer TGA 4000 Thermogravimetric Analyzer with a computer interface. The thermal measurements were carried out in a ceramic crucible under an atmosphere of flowing N_2 gas (50 cm^3 min^{-1}) with a heating rate of 10 °C min^{-1}.

2.2. Synthesis of $[Cu_4Zr_6(\mu\text{-}O)_8(dmap)_4(OAc)_{12}]\bullet H_2O$ (1)

0.500 g (2.51 mmol) copper (II) acetate monohydrate was added to a solution of 0.820 g (2.51 mmol) of $Zr(dmap)_4$ in 20 mL of THF and was stirred for 4 hours at room temperature. All volatiles were evaporated under reduced pressure and the solid residue was dissolved in 5 mL of THF to obtain a green crystalline product in 70% yield. Mp: 255-260°C (decomposition). Microanalysis: % Anal calcd. for $C_{44}H_{86}Cu_4Zr_6N_4O_{37}$: C, 25.59; H, 4.20; N, 2.71. Found: C, 25.77; H, 4.09; N, 2.71%. IR (cm^{-1}): 3436br, 2916br, 1608s, 1563s, 1430br, 1330w, 1296s, 1168w, 1100s, 1057s, 1014s, 957w, 946w, 862w, 782s, 687s, 659w, 644s, 612w, 567s, 531br, 490w, 463w. TGA: 42-120 °C (1.00% wt. loss); 130-280 °C (18.90% wt. loss); 281-314 °C (18.80% wt. loss), 315-570 °C (10.35% wt. loss) (Residual mass of 50.95% %); (Cal. for CuO-$1.5ZrO_2$ 51.15%).

2.3. Single-crystal X-ray Crystallography

Diffraction data for the crystal of (**1**) were collected on a Bruker SMART Apex II CCD area-detector diffractometer (graphite-monochromatized Mo-K_α radiation, λ = 0.71073 Å) at 133(2) K. The orientation matrix, unit cell refinement and data reduction were all handled by the Apex2 software (SAINT integration, SADABS multi-scan absorption correction).[36] The structure was solved using direct methods in the program SHELXS-97,[37] and was refined by the full matrix least-squares method on F^2 with SHELXL-2014/7. All the non-hydrogen atoms were refined

anisotropically. All the C-bound hydrogens were placed at calculated positions and were treated as riding on their parent atoms. The water hydrogens were found in a difference Fourier map and refined with a distance restraint of O—H = 0.95 (4) Å. Drawing of the molecule was produced with XSEED. [38]

2.4. Deposition of thin films by AACVD

Copper oxide-zirconium oxide composite thin films were deposited on commercially available FTO conducting glass substrates by using an in-house designed AACVD assembly. Before carrying out the deposition, substrates were cleaned with distilled water, acetone and ethyl alcohol, then placed inside the reactor tube and furnace (CARBOLITE, Model No. 10/25/130) (6"L × 1"D) and heated up to the deposition temperature of 550 °C for 10 minutes. The deposition experiments were conducted using 20 mL of 0.1M solutions of precursor (**1)** in two different solvents viz. methanol and ethanol. In a typical deposition experiment, a precursor solution was taken in a 50mL round bottom flask which was immersed in water bath above the piezoelectric modulator of an ultrasonic humidifier (Model No. Cool Mist-plus serial No. ADV-CMP-85956). Air at a flow rate of 100 mL min^{-1} was used as the carrier gas and the flow rate was controlled by an L1X linear flow meter. The generated aerosol droplets were then transferred into the hot wall zone of the reactor by the carrier gas. Both the solvent and precursor were evaporated and the precursor vapour reached the heated substrate surface where thermally induced reactions and subsequent film deposition took place.

2.5. Thin film analysis

The XRD patterns of the thin films were recorded on a PANanalytical, X'Pert HighScore diffractometer with primary monochromatic high intensity CuK_α(λ = 1.5418 Å) radiation over

Bragg angles ranging from 10 to 90° in a step size of 0.026° while the operating voltage and current were maintained at 30kV and 40mA respectively.

The surface morphology and chemical composition of thin films were analyzed by field-emission gun scanning electron microscope (Hitachi FESEM SU 8000) equipped with an energy dispersive X-ray spectrometer EDX (INCA Energy 200, Oxford Inst.) operated at an accelerating voltage of 20 kV and a working distance of 9.2mm. X-ray photoelectron spectroscopy of thin films were studied using an ULVAC-PHI Quantera II with a 32-channel Spherical Capacitor Energy Analyzer under vacuum (1 x 10^{-6} Pa) using Monochromated Al Kα radiation (1486.8eV) and natural energy width of 680meV. The carbonaceous C 1s line (284.6 eV) was used as a reference to calibrate the binding energies.

2.6. Electrochemical studies

All the electrochemical measurements were carried out using a Princeton Applied Research, USA VersaSTAT-3 electrochemical analyzer with a conventional three-electrode system under a nitrogen atmosphere at room temperature (27 °C). The CuO-1.5ZrO_2 modified electrode was used as a working electrode, a platinum wire used as a counter electrode, and an Ag/AgCl electrode was employed as a reference electrode. All the potentials are stated against the Ag/AgCl electrode unless otherwise mentioned. The supporting electrolyte and target substrate were made up of 0.1 M KOH and 0.1 M CH_3OH, respectively.

3. Results and discussion

3.1. Synthesis and characterization of complex (1)

The conventional zirconium alkoxides usually exist in oligomeric arrangement formed via μ-alkoxide bridges and are thus found as insoluble, nonvolatile and thermally less stable species.[34, 35] It is worth noticing that steric demand and coordinative flexibility of the ligand system have a

great influence on the aggregation and volatility of the precursor complexes. Therefore, the modification of zirconium alkoxides by their reaction with aminoalcohols is an effective synthetic strategy to convert them into low nuclearity, volatile and soluble metal alkoxides derivatives.[39] Aminoalcohols are simple derivatives of alcohols from which the hydrogen atoms of the alkyl or alkene groups have been replaced by amino or N-alkyl substituted amino groups. Such reagents because of their multidentate behavior and/or steric bulk are able to reduce the oligomerization of the metal alkoxides and improve their capability for CVD applications.

As reported earlier[10-15] the reaction of metal alkoxides or aminoalkoxides with metal acetate is a promising method to design heterobimetallic complex for the deposition of thin films of a desired oxide material. This type of synthetic strategy aims to coordinatively saturate each metal center by the use of chelating ligands such as carboxylate and a functionalized alcohol which strictly restrict the resulting complexes into a molecular regime and enhance their stability, solubility, volatility and shelf life. Metal alkoxides and carboxylates generally react with one another by the elimination of an ester as a volatile by-product, but in the reaction observed here, it is more likely that the oligomeric oxo complex was formed through hydrolysis from the hydrated starting materials in combination with the loss of acetate and dmapH ligands. However, such reactions can occur under very mild conditions (room temperature and nonpolar solvents), and thus the complexes can be synthesized by simple mixing of the starting materials in an appropriate solvent. The reactions between $Cu(OAc)_2 \cdot H_2O$ with $Zr(dmap)_4$ demonstrate these features. These reactions proceed smoothly and quantitatively in hydrocarbon solvents over a period of 1 or 2 h with progressive dissolution of the acetate. The unreacted excess of metal acetate is easily removed by filtration, and the complexes can be crystallized out almost quantitatively from the filtrate. Thus the complex $[Cu_4Zr_6(\mu\text{-}O)_8(dmap)_4(OAc)_{12}] \bullet H_2O$ (**1**), was

prepared in yield of 70% by reacting appropriate amounts of tetrameric *N,N*-dimethylaminopropanolato Zr(IV) with Cu(II) acetate in THF at room temperature. The compound was found to be soluble in polar solvents and solubility was found to be poorer in solvents like benzene and toluene. The compound was stable under ambient conditions. The microanalysis of complex (**1**) was found to be consistent with the empirical formula $C_{44}H_{86}Cu_4Zr_6N_4O_{37}$. The appearance of a broad band at 3436 cm^{-1} is assignable to the ν(O–H) vibration of the solvated water molecules present in (**1**)**.** The IR spectrum of complex (**1**) shows the presence of characteristic vibrations of both carboxylato and aminoalcoholato functional groups attached to the copper and zirconium atoms. In complex (**1**), the different modes of the carboxylate binding, namely bidentate bridging, bridging-monodentate and monodendate terminal coordination of the acetate ligand have also been established from the IR spectrum. The two strong bands at 1563 and 1430 cm^{-1} are due to the asymmetric and symmetric stretching vibrations of a bridging acetate functionality of the ligand, respectively. The difference of Δ = 133 cm^{-1} between the asymmetric and symmetric stretching vibrations is attributed to the bidentate bridging of the acetate group.[40] In addition, the asymmetric and symmetric carboxylate stretches are observed at 1608 and 1330 cm^{-1} respectively, (Δ = 278 cm^{-1}), suggesting the presence of bridging monodentate coordination mode of the acetate ligand. Generally the order of Δ, ($\Delta = \nu_{as(COO^-)} - \nu_{s(COO^-)}$), for metal carboxylates is of the order Δ(bridging) < Δ(monodentate). The lower Δ value (133 cm^{-1}) compared to that of higher value (278 cm^{-1}) strongly suggest the presence of bidentate bridging along with the bridging monodentate coordination.[41] The absorptions at the low frequencies of 531 and 463 cm^{-1} are probably due to M–O and M–N stretching vibrations respectively.[42]

3.2. Single crystal X- ray structure of complex (1)

The crystal structure of complex $[Cu_4Zr_6(\mu\text{-}O)_8(dmap)_4(OAc)_{12}]$ (**1**) is depicted in Fig. 1 and a schematic drawing is shown in Fig. 2. Crystal data and refinement parameters are given in Table 1. Table 2 lists the coordination bond lengths for the structure.

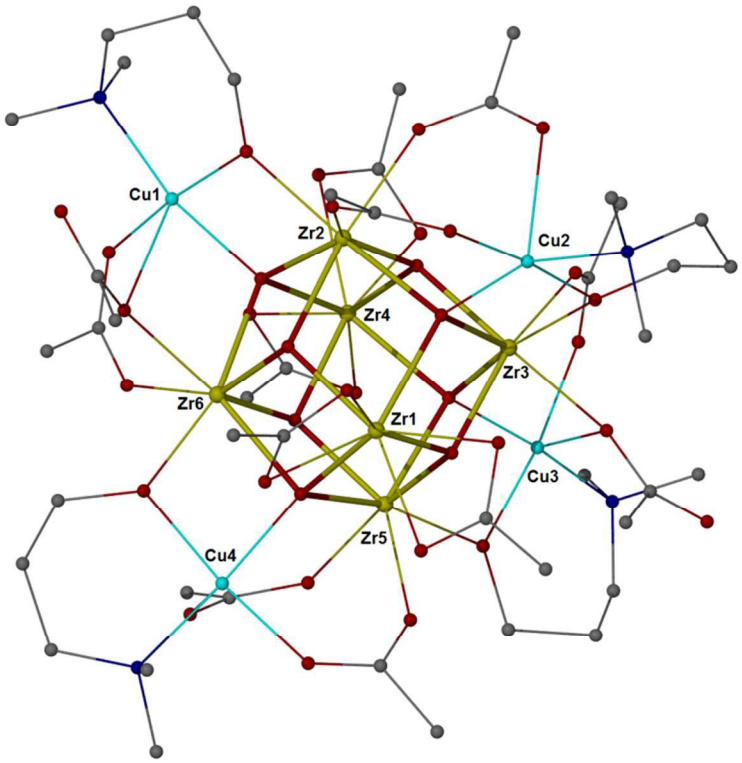

Figure 1: Crystal structure of complex $[Cu_4Zr_6(\mu\text{-}O)_8(dmap)_4(OAc)_{12}]$ (**1**). H-atoms and the hydration water molecules are omitted for clarity. Zr: golden, Cu: turquoise, O: red, N: blue, C: dark grey.

In the molecule, six octahedrally arranged Zr^{IV} atoms are bridged by eight oxides forming a rhombic dodecahedral Zr_6O_8 cage. The cage is surrounded by four tetrahedrally located Cu^{II} atoms. Four of the cage O-atoms are of μ_4-type, each bridges one Cu^{II} and three Zr^{IV} centers. The other four oxides are μ_3 and link only three Zr^{IV} centers. The Zr-(μ_4-O) distances range between 2.159-2.208 Å, which are slightly longer than Zr-(μ_3-O) bond lengths (2.055-2.088 Å). Two of the Zr centers (Zr1 and Zr4) are eight coordinated by four cage O-atoms and two chelating acetato ligands. The other four Zr centers are seven coordinated by four cage O-atoms, and three

O atoms from one dmap and two acetato ligands. Each Cu atom is coordinated by one cage O-atom, one *N,O*-chelating dmap and two bridging acetato ligands in a distorted square-pyramidal geometry. In the crystal, hydration water molecules link the neighbouring complex molecules through O-H…O interactions.

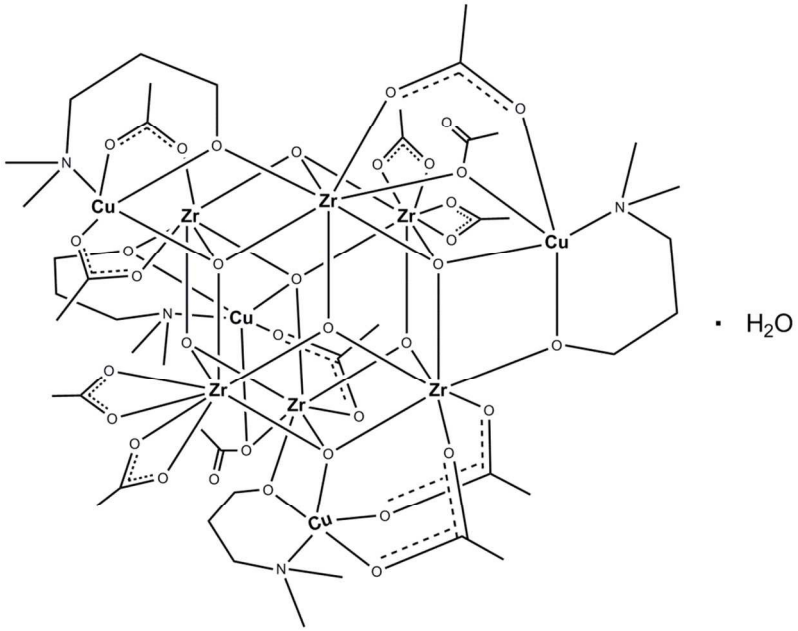

Figure 2: Schematic diagram of complex $[Cu_4Zr_6(\mu\text{-}O)_8(dmap)_4(OAc)_{12}] \cdot H_2O$, (**1**).

<Table 1>

<Table 2>

3.3. Thermal analysis of complex (1)

The nature of thermolysis of complex (**1**) was examined by thermogravimetric (TG), derivative thermogravimetric (DTG) and differential scanning calorimetric (DSC) analyses performed under an inert nitrogen atmosphere with a flowing rate of 25 cm^3 min^{-1} and a heating rate of 10 °C min^{-1} and results are plotted in Fig. 3. The TG/DTG profiles (Fig. 3) indicate that

complete thermal decomposition of complex (**1**) proceeds in four distinct steps of weight loss which appear as endothermic and exothermic steps by DSC curve. The maximum heat intake sequentially occurs at 85, 267, 293 and 332 °C representing a weight loss of 1.00, 18.90, 18.80 and 10.35% correspondingly.

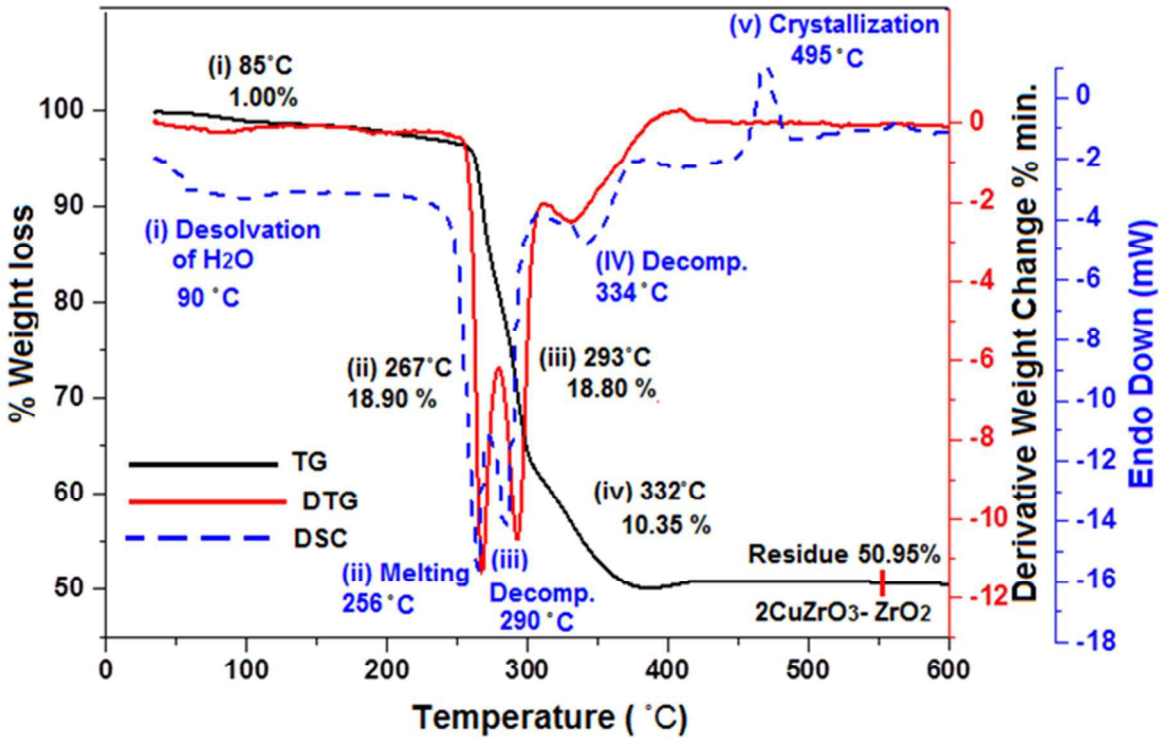

Figure 3: TG (black), DTG (red) and DSC (blue) profiles showing thermal decomposition of complex (**1**) as a function of temperature.

DSC (blue curve in Fig. 3) recognizes these weight loss stages in form of endothermic peaks at 90, 256, 290 and 334 ˚C and designates as the desolavtion of water molecules, melting and decomposition phases, respectively occurring in complex (**1**) during its heat treatment process. The weight loss featured in Fig. 3 terminates at 500 °C providing stable residues of 50.95% of its original mass which is in reasonable agreement with the formation of the expected 1:1.5 of CuO:

ZrO_2 (51.15%) composite oxide material from (**1**). The exothermic peak appearing at 495 ˚C in DSC is attributed with the crystallization process occurring in the residual CuO-1.5ZrO_2 material.

3.4. XRD

As the thermogravimetric analysis confirms the possibility of complex (**1**) to be used as SSMP, thus, solution of complex (**1**) in two different solvents methanol and ethanol was prepared individually and employed in AACVD to observe the formation of composite oxide thin films at a temperature of 550 ˚C on FTO conducting glass substrate using air as carrier gas. In order to determine the nature and chemical formula of the crystalline deposit, the thin films were characterized by XRD and the resultant X-ray diffraction patterns are presented in Fig. 4. A careful matching of the XRD patterns with the standard inorganic crystal structure database available in PANalytical X'Pert HighScore Plus" software identifies the growth of tenorite CuO (98-001-6025)[43] and zirconium oxide-Ht ZrO_2 (98-005-3998)[44] phases in the deposit product. The as-synthesized tenorite copper oxide crystallizes in the monoclinic crystal system with cell parameters a = 4.684, b = 3.423, c = 5.129 Å; $\alpha = \gamma = 90^\circ$ and $\beta = 99.54^\circ$ and produced peaks at 2θ = 35.55, 38.80, 48.80, 58.50, 66.30, 68.13, and 80.22˚ as observed by their Miller indices (11-1), (111), (20-2), (202), (31-1), (220) and (11-4) respectively. The zirconium oxide-Ht possesses a cubic crystal system with space group *Fm-3m* with cell parameters of $a = b = c$ = 5.100 Å; $\alpha = \beta = \gamma = 90.0^\circ$ and showed crystalline peaks at 2θ = 30.33˚ (111), 35.15˚ (002), 50.60˚ (022), 60.25˚ (113), 63.0˚ (222), 74.50˚ (004), 82.30˚ (133) and 85.0˚ (024). The X-ray diffractograms also demonstrate the overlapped peaks between CuO and SnO_2 at 2θ values of 51.0˚, 57.8˚, 61.68˚ and 65.84˚. In the X-ray diffractograms the reflections related to CuO are labeled as "X" while ZrO_2 reflections are marked by "Y". The peaks indicated by "*" correspond to SnO_2 of

crystalline FTO substrate. Both XRD patterns are dominating by peak at 2θ = 30.3˚. No possible crystalline impurities such as metallic copper or other phases of copper oxides or zirconium oxides were detected from these XRD patterns.

The XRD qualitative phase analysis reveals that all the copper oxide-zirconia composite films deposited from two different solvents have similar crystalline phases of tenorite CuO and a zirconium oxide-Ht. Subsequently, the XRD semi-quantification analysis was applied on each X-ray diffractogram to measure the proportion of crystallinity of each phase in the crystalline composite product. The crystalline composition of CuO-1.5ZrO_2 deposit obtained from methanol is poised at 30% CuO and 70% ZrO_2 respectively (inset Fig. 4a). However the film deposited from ethanol contains the crystalline contents of 53% CuO and 47% ZrO_2 respectively. It is worth emphasizing that the films obtained from two different solvents differ in terms of their percentage crystalline composition of the phases, however the overall phase composition of 1:1.5 for CuO:ZrO_2 can be further confirmed from energy dispersive X-ray and XPS analyses.

The disparities in crystalline composition of the films prepared from different solvents propose that solvents play a key role in dictating the crystalline phases of the films grown on the substrate surface by AACVD, and not just as a transport medium. In aerosol deposition, solvents play an important role in the determination of the extent of a reaction. The precursor can react differently in various solvents in the gas phase which may lead to the formation of different intermediates and thus to different phases of the deposit. There have been similar reports whereby a variety of solvents have been used to alter the phase composition of materials using AACVD technique.[45,46]

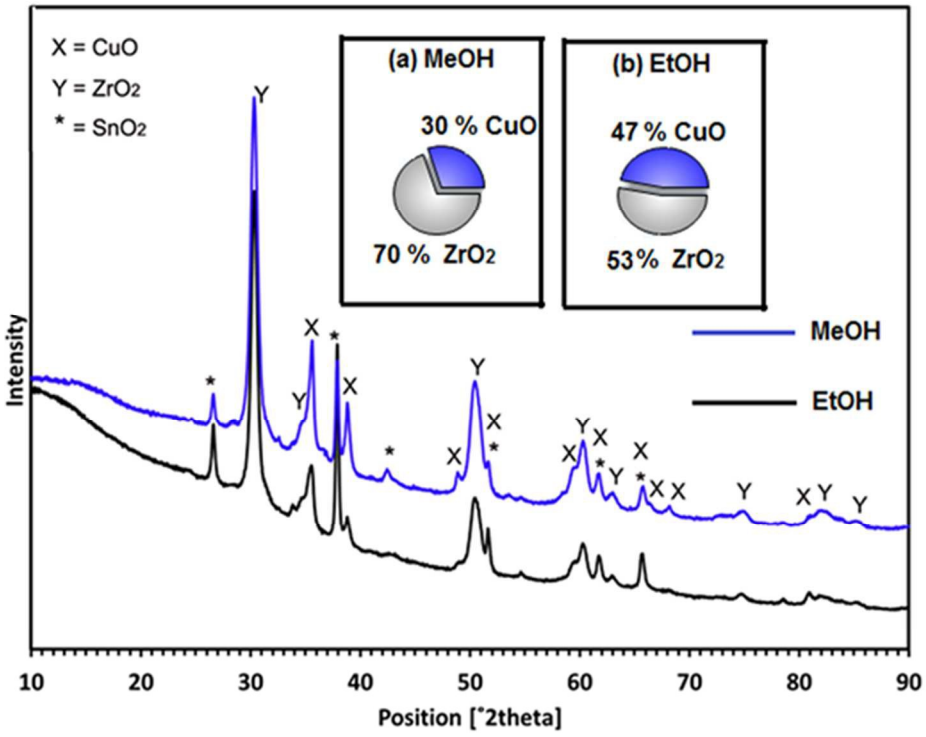

Figure 4: X-ray diffractograms of the CuO-1.5ZrO_2 composite thin films prepared from solutions of (**1**) in methanol (blue line) and ethanol (black line) on FTO glass at 550 °C in air ambient; Inset shows the phase compositions of the CuO-1.5ZrO_2 composite films from (**a**) methanol: 30% tenorite CuO and 70% ZrO_2; (**b**) ethanol: 47% CuO and 53% ZrO_2.

3.5. SEM/EDX analysis

The surface topography of the CuO-1.5ZrO_2 composite oxide thin films grown from 0.1 M (20 mL) solution of precursor (**1**) in methanol and ethanol were examined by scanning electron microscopy (SEM) and the developed microstructures are presented in Fig. 5.

Fig. 5(**a**) shows that the surface architecture of the film obtained from methanol solution is composed of well-defined and orderly packed microspheres having a size range of 0.2–0.7 μm. Fig. 5 (**a**) also demonstrates that textures of some microspheres belong to highly wrinkled morphology while the other type displays a smooth and simple design.

Fig. 5(**b**) shows the surface morphology of CuO-1.5ZrO_2 composite thin films grown from the ethanol solution of (**1**). The film consists of interconnected spherical objects of

heterogeneous design, shape and size which are grown in the vertical direction of the substrate plane. One type of microspherical object attain donuts shape structure while the others are round ball shaped entities of size range 0.5-1.3μm.

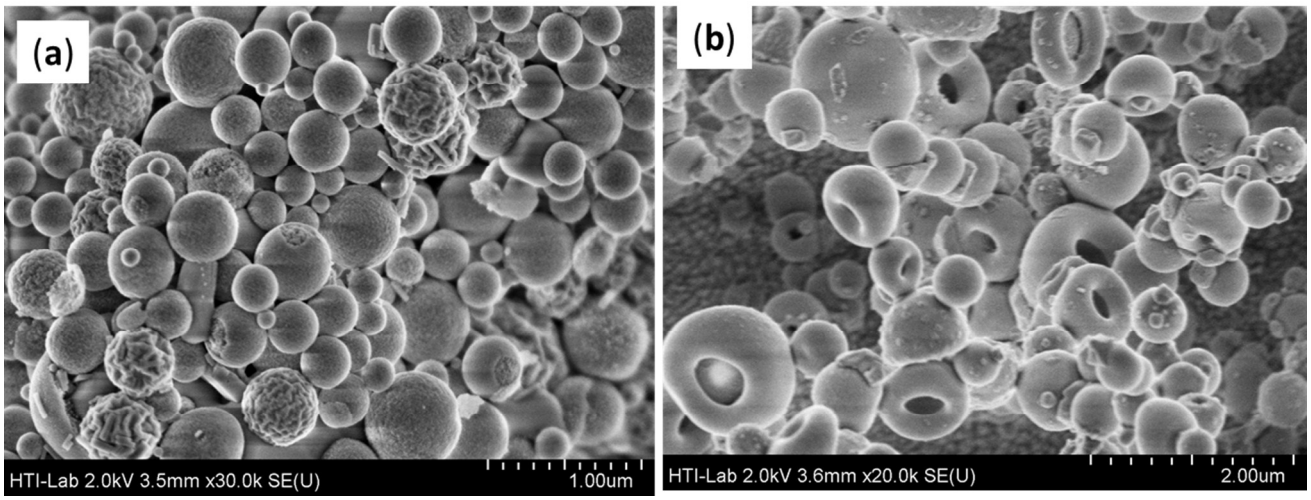

Figure 5: SEM images of CuO–1.5ZrO_2 composite oxide films deposited on FTO glass substrate at 550 ˚C from solution of precursor (**1**) in (**a**) methanol (**b**) ethanol.

The mechanism of formation of different design, shape and size microspheres thin films by AACVD is mainly controlled by homogenous and heterogeneous type of reactions occurring between precursor gaseous intermediate and substrate surface. The gas phase reaction pathways are significantly inveigled by the type of solvent used and are explicated well by us and others previously.[47,48] In the present scenario we used two different types of solvents such as methanol and ethanol which because of their different physical properties (densities, boiling points and enthalpies) affect the course of gas phase reactions and help in building microsphere structures of different shape and architectures.

The elemental composition of $CuO–1.5ZrO_2$ composite oxide thin films were determined by energy dispersive X-ray (EDX) analysis and are presented in Fig. S1 and S2. The EDX analysis executed on several randomly selected large regions reveal that the metallic ratio of Cu:Zr in the films is close to 1:1.5 confirming the retention of the same metallic ratio in the films as found in complex (**1**).

Further the composite nature of the $CuO–1.5ZrO_2$ films invented from methanol and ethanol solutions of precursor (**1**) was established from EDX mapping (Fig. 6 (a and b)) which reveals that Cu, Zr and O atoms are evenly distributed throughout the films matrix.

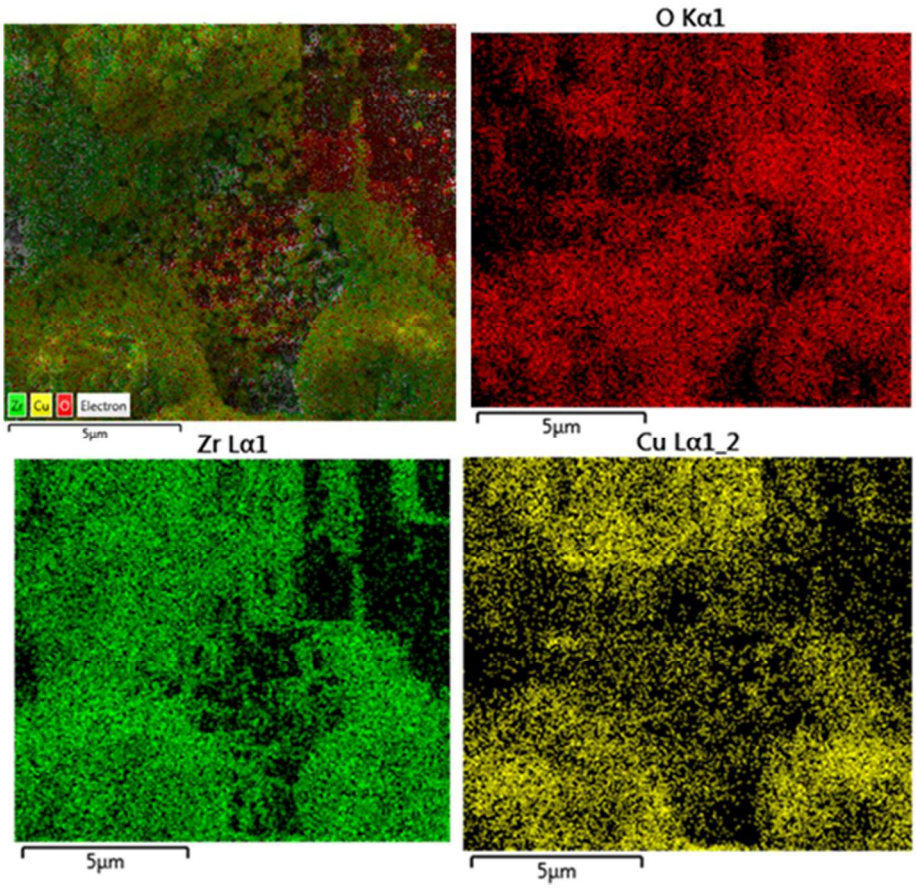

Figure 6a: Elemental map showing the distribution of Cu, Zr and O elements in $CuO–1.5ZrO_2$ composite thin film deposited from methanol solution of precursor (**1**).

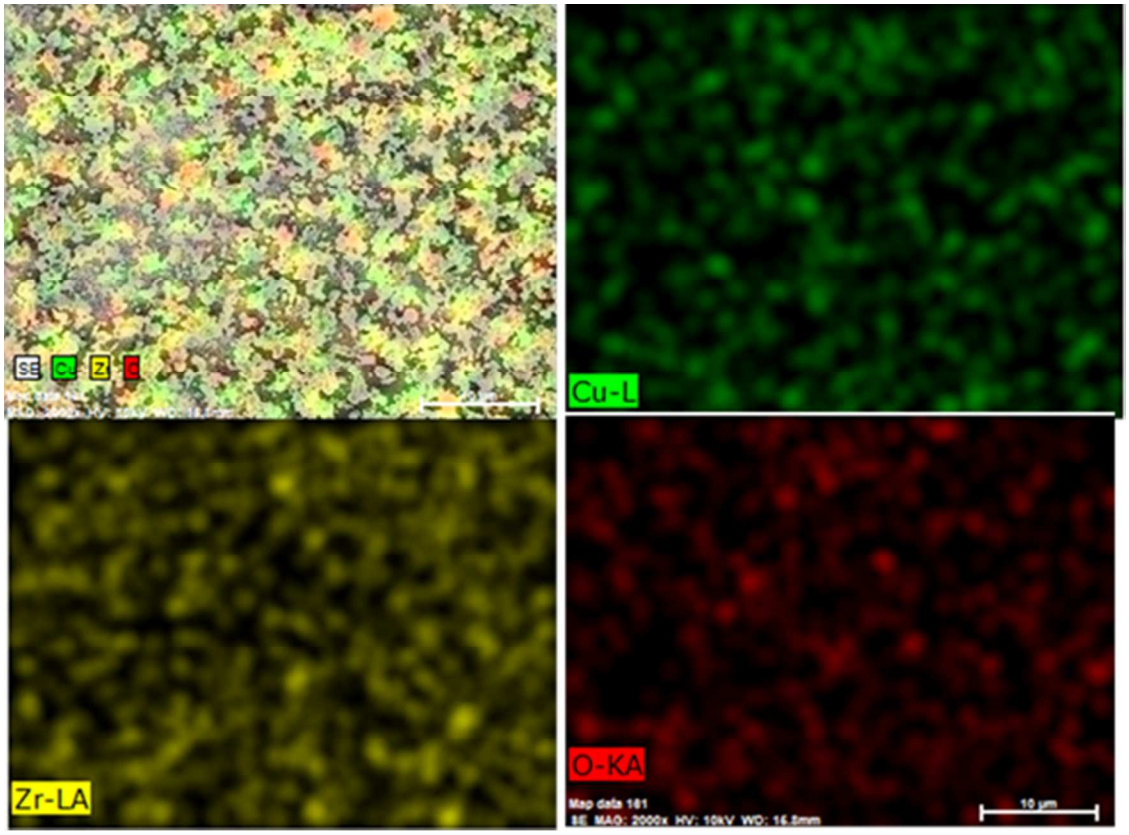

Figure 6b: Elemental map showing the distribution of Cu, Zr and O elements in CuO–1.5ZrO_2 composite thin film deposited from ethanol solution of precursor (**1**).

3.6. XPS

The XPS analysis was employed to determine the surface composition and chemical states of the Cu, Zr, and O elements in CuO-1.5ZrO_2 composite oxide thin films prepared from methanol and ethanol solutions of precursor (**1**). The wide scan spectra in Figure 7(a) shows the binding energy peaks at 181.9, 285.4, 529.9 and 933.4 eV which are attributed to Zr 3d, C 1s, O 1s and Cu 2p respectively. In the high resolution Zr 3d spectra (Figure 7(b)), binding energies of 182.0 and 184.5 eV are indicative of Zr 3d5/2 and Zr 3d3/2 respectively which correspond to Zr^{4+} and is in good agreement with the published data for ZrO_2.[26,49] Meanwhile, the peak at 530.3eV is an evidence of O1s in ZrO_2 and CuO (Figure 7(c)). The Cu 2p peak of the CuO-1.5ZrO_2 is shown in Figure 7(d). The Cu 2p3/2 is allocated at 934.5eV with a shakeup satellite peak at about 942.8eV

and Cu 2p1/2 lies at 953.6eV with a satellite peak at about 962.5eV, which is consistent with earlier reports.[28,50] The presence of shakeup satellite features for Cu 2p rules out the possibility of Cu_2O phase presence. The gap between Cu 2p1/2 and Cu 2p3/2 is about 20eV, which is in agreement with the standard CuO spectrum.[51]

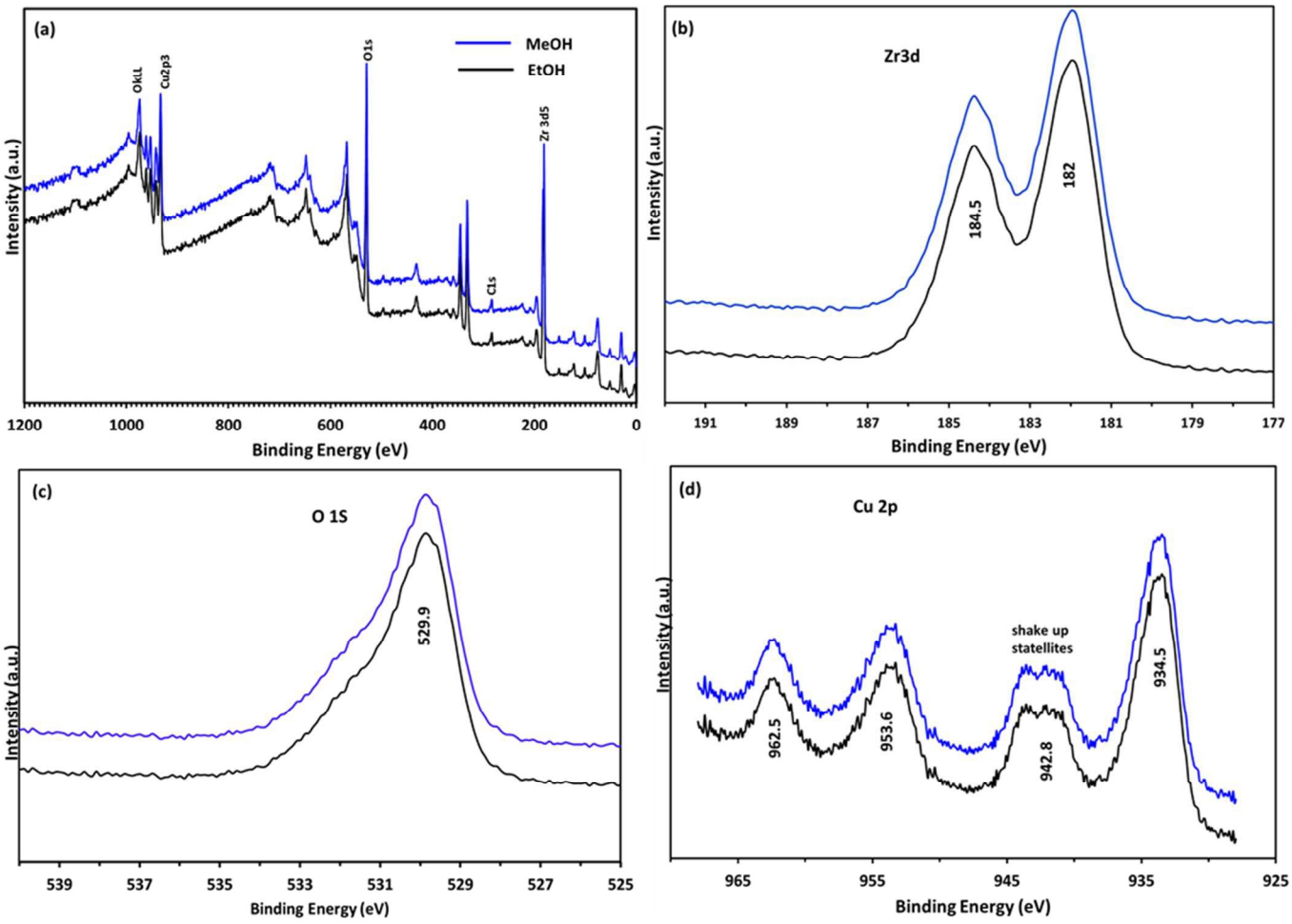

Figure 7: (**a**) wide scan XPS spectra of CuO-1.5ZrO_2 composite thin films prepared from methanol (blue line) and ethanol (black line); High resolution spectra CuO-1.5ZrO_2 for (**b**) Zr 3d (**c**) O 1s (**d**) Cu 2p

3.7. Electrocatalytic oxidation of methanol at CuO-1.5ZrO_2 composite thin film

The CuO-1.5ZrO_2 thin film fabricated from methanol solution exhibits better connectivity pattern and compact microstructure, therefore the film from methanol solution was further investigated toward the electrocatalytic oxidation of methanol. In order to study the electrocatalytic activity, a cyclic voltammogram was recorded in the presence of 0.1 M CH_3OH and 0.1 M KOH at a scan rate of 50 mVs^{-1} for the CuO-1.5ZrO_2 composite oxide thin film modified Pt electrode, and results are shown in Fig. 8(b). For comparison purpose, cyclic voltammograms were also recorded for bare Pt electrode under identical experimental conditions (Fig. 8(a)). It can be seen that the CuO-1.5ZrO_2 composite oxide thin film modified Pt electrode showed the oxidation peak current of 14 µA which is ~3.5-fold higher than that of the bare Pt electrode (4 µA).

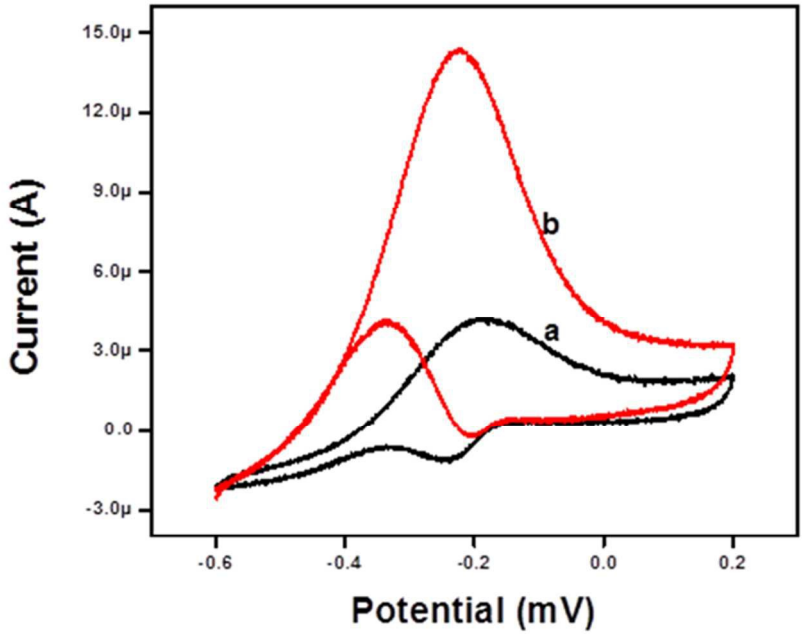

Figure 8: Cyclic voltammograms observed for the (**a**) bare Pt and (**b**) CuO-1.5 ZrO_2 composite oxide film modified Pt electrode in the presence of 0.5 M CH_3OH and 0.1 M KOH at a scan rate of 50 mVs^{-1}.

It is observed that the CuO-1.5ZrO_2 composite electrode showed a higher electrocatalytic oxidation current during forward (14 μA) and backward (4 μA) scans compared to the bare Pt electrodes. The peak currents observed during the forward and reverse scans were due to the methanol oxidation and removal of the residual carbonaceous species formed in the forward scan, respectively.[52,53] The higher electrocatalytic activity of the CuO-1.5ZrO_2 modified electrode compared with bare Pt electrode was attributed to the catalytic properties of copper oxide- zirconia composite material and tightly packed spherical architecture of the film.

3.8. Influence of experimental parameters on the electrocatalytic oxidation of methanol

The influence of scan rate on the electrocatalytic oxidation of methanol was studied by varying the scan rates from 10 to 350 mV/s for the CuO-1.5 ZrO_2 composite oxide film modified Pt electrode in the presence of 0.5 M CH_3OH and 0.1 M KOH, and the results are shown in Fig. 9. While increase the scan rate the oxidation peak current also increased due to the enhanced the electron movement between electrode and electrolyte interface.

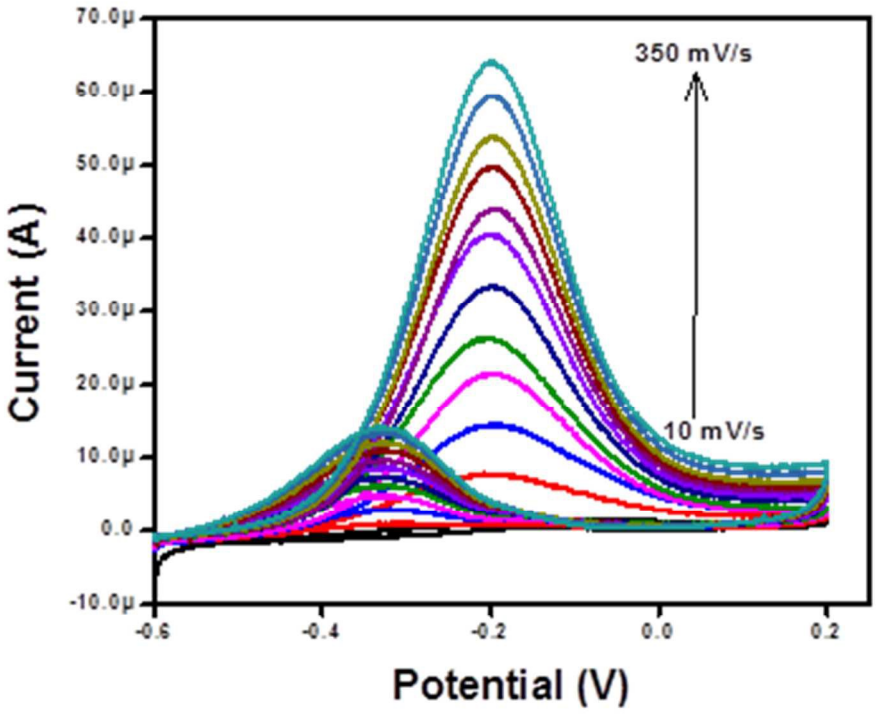

Figure 9: CV recorded for the CuO-1.5ZrO_2 composite oxide film modified Pt electrode in presence of 0.5 M CH_3OH and 0.1 M KOH at different scan rates in range of 10–350 mVs^{-1}.

The CuO-1.5ZrO_2 composite oxide film modified Pt electrode showed a linearly increase anodic peak current towards forward and backward oxidation peak. This suggests that the electrocatalytic oxidation of methanol at the CuO-1.5ZrO_2 composite oxide film modified Pt electrode is a diffusion-controlled process.

In practical application of direct methanol fuel cells (DMFC), methanol concentration plays a vital role. In this regard effect of methanol concentration was studied by varying the concentration of methanol in the presence of CuO-1.5ZrO_2 composite oxide film modified Pt electrode at a scan rate of 50 mVs^{-1} in the presence of 0.1 M KOH and the results are shown in Fig. 10. It can be noticed that anodic peak current increases and the anodic peak potential have a slightly shifted to positive potential while increase in the methanol content due to the saturation of active catalytic sites at the CuO-1.5ZrO_2 composite oxide film modified Pt electrode surface.

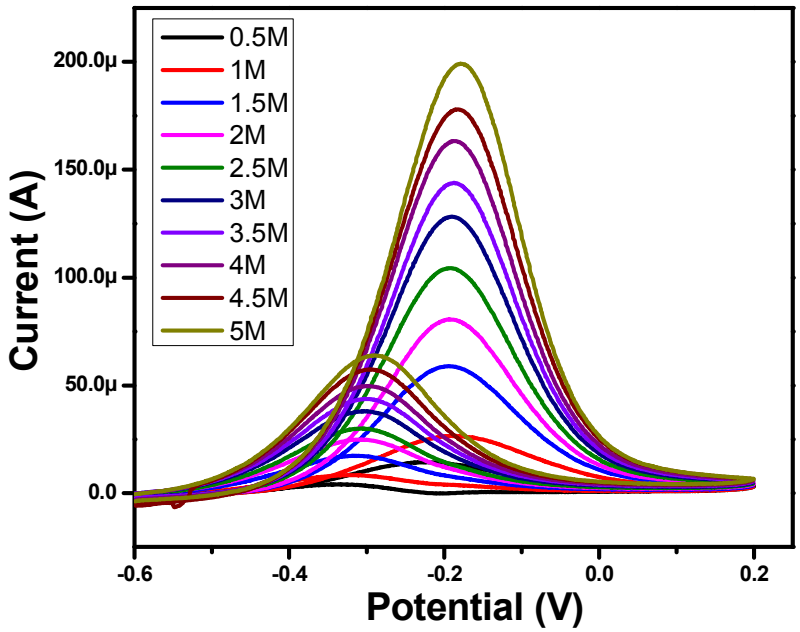

Figure 10: CV recorded for the CuO-1.5ZrO_2 composite oxide film modified Pt electrode at scan rate 50 mVs^{-1} in presence of 0.1 M KOH and various concentrations of CH_3OH.

Table 3 shows the comparison of electrocatalytic performances of some metal oxides catalysts towards methanol oxidation.

< **Table 3** >

It is widely accepted that CO species produced in the process of methanol electrooxidation are the main poising intermediate that slow down the oxidation kinetics.[54] This problem can be solved by using metal oxides (TiO_2, ZrO_2 and MoO_2) which can effectively promote the electrocatalytic oxidation of methanol and show perfect tolerance to CO poisoning.[54] At the same time the low price and abundance of metal oxide can help to reduce the cost of DMFC. Further, to improve the performance of electrocatalytic oxidation of methanol, carbon nanotubes (CNTs) and reduced graphene oxide (rGO) have been frequently used as the support which provides large network for collecting electrons from oxidation process thereby assisting efficient current generation. It can be seen from table 3 that the metal oxide composite with CNTs and rGO showed higher methanol oxidation current than the present catalyst, CuO-1.5ZrO_2. However, considering the high cost of Pt metals, present catalyst prepared from AACVD technique is suitable alternative to Pt free electrocatalyst for the methanol oxidation due to the low cost and ease of fabrication.

4. Conclusions

In summary, we have presented a synthetic protocol for the preparation of heteronuclear complex $[Cu_4Zr_6(\mu\text{-}O)_8(dmap)_4(OAc)_{12}]\bullet H_2O$ (**1**) by reacting $Cu(OAc)_2\cdot H_2O$ with modified

zirconium aminoalkoxide $Zr(dmap)_4$ in THF. The structural elucidation shows that the molecule contains a $Zr_6(\mu\text{-}O)_8$ core attached to four Cu^{II} ions. The pyrolysis of complex (**1**) yields a composite mixture of 1:1.5 ratio of CuO: 1.5 ZrO_2 at 550 ˚C. The exceptionally good solubility and solution stability of complex (**1**) in methanol and ethanol solvents allows its implementation as a single source precursor in aerosol assisted chemical vapor deposition technique for the fabrication of composite oxide thin film. The powder X-ray diffraction, scanning electron microscopy, energy dispersive X-ray and photoelectron spectroscopic analyses of the developed thin films show the growth of advanced composite oxides of CuO-1.5 ZrO_2 with round-shaped object of grain size ranging from 0.3-0.7 μm. The electrocatalytic activity of CuO-1.5ZrO_2 composite oxide film was studied toward methanol oxidation in an alkaline medium and it showed high oxidation peak current of 14 μA during a forward scan which is ~3.5-fold higher than the bare Pt electrode. In addition, the CuO-1.5ZrO_2 composite electrode showed a higher electrocatalytic oxidation current during forward (14 μA) and backward (4 μA) scans compared to the bare Pt electrodes. The ease of fabrication, high electrocatalytic activity of composite oxide could make it potential candidate for direct methanol fuel cells application.

Acknowledgements

The authors acknowledge funding from UMRG, High-Impact Research scheme: UMRG scheme grant number: RP007A-13AET, HIR: UM.C/625/1/HIR/242.

Supplementary data

CCDC 1401618 contains the supplementary crystallographic data for this paper. These data can be obtained free of charge via http://www.ccdc.cam.ac.uk/conts/retrieving.html, or from the Cambridge Crystallographic Data Centre, 12 Union Road, Cambridge CB2 1EZ, UK; fax: (+44) 1223 336 033; or e-mail: deposit@ccdc.cam.ac.uk.

Electronic Supplementary Information (ESI) available: [Microanalysis result, Energy dispersive X-ray spectra]. See DOI: 10.1039/b000000x/

References

1. S. Szafert, Ł. John and P. Sobota, Dalton Trans., 2008, 6509-6520.
2. Ł. John and P. Sobota, *Acc. Chem. Res.*, 2013, **47**, 470-481.
3. I. Bulimestru, S. Shova, N. Popa, P. Roussel, F. Capet, R.-N. Vannier, N. Djelal, L. Burylo, J.-P. Wignacourt and A. Gulea, *Chem. Mater.,* 2014, **26,** 6092-6103.
4. S. Mishra and S. p. Daniele, *Chem. Rev*, 2015.
5. T. Ould-Ely, J. H. Thurston and K. H. Whitmire, *Comptes Rendus Chimie*, 2005, **8**, 1906-1921.
6. Y. Deng, S. Tang and S. Wu, *Solid State Sci.,* 2010, **12**, 339-344.
7. Y. Deng, Q. Lv, S. Wu and S. Zhan, Dalton Trans., 2010, **39**, 2497-2503.
8. J. H. Thurston, D. Trahan, T. Ould-Ely and K. H. Whitmire, *Inorg. Chem.,* 2004, **43**, 3299-3305.
9. J. H. Thurston, T. O. Ely, D. Trahan and K. H. Whitmire, *Chem. Mater.,* 2003, **15**, 4407-4416.
10. M. Sultan, A. A. Tahir, M. Mazhar, K. U. Wijayantha and M. Zeller, Dalton Trans., 2011, **40**, 7889-7897.
11. M. Sultan, A. A. Tahir, M. Mazhar, M. Zeller and K. U. Wijayantha, *New J. Chem.*, 2012, 36, 911-917.
12. S. Ahmed, M. A. Mansoor, M. Mazhar, T. Söhnel, H. Khaledi, W. J. Basirun, Z. Arifin, S. Abubakar and B. Muhammad, Dalton Trans., 2014, **43**, 8523-8529.
13. S. Ahmed, M. A. Mansoor, W. J. Basirun, M. Sookhakian, N. M. Huang, L. K. Mun, T. Söhnel, Z. Arifin and M. Mazhar, *New J. Chem.*, 2015.
14. M. Shahid, M. Hamid, M. Mazhar, J. Akhtar, M. Zeller and A. D. Hunter, *Inorg. Chem. Commun.,* 2011, **14**, 288-291.
15. M. Shahid, M. Mazhar, M. Hamid, P. O'Brien, M. A. Malik and J. Raftery, *Inorg. Chimica Acta* 2010, **363**, 381-386.

16. R. K. Dubey, *Transition Metal Chemistry*, 1993, **18**, 243-247.
17. J. A. Samuels, B. A. Vaartstra, J. C. Huffman, K. L. Trojan, W. E. Hatfield and K. G. Caulton, *J. Am. Chem. Soc.,* 1990, 112, 9623-9624.
18. J. A. Samuels, W.-C. Chiang, J. C. Huffman, K. L. Trojan, W. E. Hatfield, D. V. Baxter and K. G. Caulton, *Inorg. Chem.,* 1994, 33, 2167-2179..
19. M. A. Ehsan, H. Khaledi, Z. Arifin and M. Mazhar, *Polyhedron*, 2015, 98, 190-195.
20. P. Tian, Y. Wei, M. Ye and Z. Liu, *ACS Catalysis*, 2015, **5**, 1922-1938.
21. X. Guo, D. Mao, G. Lu, S. Wang and G. Wu, *J. Catal.,* 2010, 271, 178-185.
22. R. Raudaskoski, E. Turpeinen, R. Lenkkeri, E. Pongrácz and R. Keiski, *Catal. Today* 2009, 144, 318-323.
23. Y. Zhang, C. Chen, X. Lin, D. Li, X. Chen, Y. Zhan and Q. Zheng, *Int. J. Hydrogen Energy* 2014, 39, 3746-3754.
24. S. Pradhan, A. S. Reddy, R. Devi and S. Chilukuri, *Catal. Today,* 2009, 141, 72-76.
25. Z. Liu, M. D. Amiridis and Y. Chen, *J. Phys. Chem. B,* 2005, 109, 1251-1255.
26. J. Huang, S.-R. Wang and S.-H. Wu, *J. Dispersion Sci. Technol.,* 2010, 31, 1469-1473.
27. S. Wang, D. Mao, X. Guo, G. Wu and G. Lu, *Catal. Commun.,* 2009, 10, 1367-1370.
28. L.-C. Wang, Q. Liu, M. Chen, Y.-M. Liu, Y. Cao, H.-Y. He and K.-N. Fan, *J. Phys. Chem. C*, 2007, 111, 16549-16557.
29. Y. Zhang, Y. Zhan, C. Chen, Y. Cao, X. Lin and Q. Zheng, *Int. J. Hydrogen Energy*, 2012, 37, 12292-12300.
30. C. A. Franchini, A. M. D. de Farias, E. M. Albuquerque, R. dos Santos and M. A. Fraga, *Appl. Catal., B* 2012, 117, 302-309.
31. P. Graf, D. De Vlieger, B. Mojet and L. Lefferts, *J. Catal.,* 2009, 262, 181-187.
32. M. Sivakumar, A. Gedanken, Z. Zhong and L. Chen, *New J. Chem.*, 2006, 30, 102-107.
33. K. V. Chary, G. V. Sagar, C. S. Srikanth and V. V. Rao, *J. Phys. Chem. B*, 2007, 111, 543-550.
34. P. Bharara, V. Gupta and R. Mehrotra, *Synthesis and Reactivity in Inorganic and Metal-Organic Chemistry*, 1977, 7, 537-546.
35. J. S. Na, D.-H. Kim, K. Yong and S.-W. Rhee, *J. Electrochem. Soc.,* 2002, 149, C23-C27.
36. B. A. I. Bruker APEX2 and SAINT, Madison, WI, USA, 2007.

37. G. M. Sheldrick, *Acta Crystallogr., Sect. A: Found. Crystallogr.,* 2008, 64, 112.
38. L. J.Barbour, *J. Supramol. Chem.*, 2001, 1, 189-191.
39. K. Fleeting, A. Jones, D. Otway, A. P. White and D. Williams, *J. Chem. Soc., Dalton Trans.,* 1999, 2853-2859.
40. A. Patra, T. K. Sen, R. Bhattacharyya, S. K. Mandal and M. Bera, *RSC Advances*, 2012, 2, 1774-1777.
41. G. Deacon and R. Phillips, *Coord. Chem. Rev.,* 1980, 33, 227-250.
42. M. Hamid, A. A. Tahir, M. Mazhar, K. C. Molloy and G. Kociok-Köhn, *Inorg. Chem. Commun.,* 2008, 11, 1159-1161.
43. L. J. Norrby and *S. Asbrink, Acta Crystallographica B* 1970, **26**, 8 - 15.
44. J. Boehm, *Golden Book of Phase Transitions, Wroclaw,*, 2002, 1, 1 – 123.
45. C. Edusi, G. Sankar and I. P. Parkin, *Chem. Vap. Deposition*, 2012, 18, 126-132.
46. M. A. Ehsan, H. Khaledi, A. Pandikumar, P. Rameshkumar, N. M. Huang, Z. Arifin and M. Mazhar, *New J. Chem.*, 2015.
47. A. A. Tahir, H. A. Burch, K. U. Wijayantha and B. G. Pollet, *international journal of hydrogen energy*, 2013, **38**, 4315-4323.
48. M. A. Ehsan, H. N. Ming, M. Misran, Z. Arifin, E. R. Tiekink, A. P. Safwan, M. Ebadi, W. J. Basirun and M. Mazhar, *Chem. Vap. Deposition*, 2012, **18**, 191-200.
49. K. V. Chary, G. V. Sagar, D. Naresh, K. K. Seela and B. Sridhar, *J. Phys. Chem. B*, 2005, **109**, 9437-9444.
50. L. Zhu, M. Hong and G. W. Ho, *Nano Energy*, 2015, **11**, 28-37.
51. M. A. Dar, S. H. Nam, Y. S. Kim and W. B. Kim, *J. Solid State Electrochem.*, 2010, **14**, 1719-1726.
52. S. Sharma, A. Ganguly, P. Papakonstantinou, X. Miao, M. Li, J. L. Hutchison, M. Delichatsios and S. Ukleja, *J. Phys. Chem. C*, 2010, **114**, 19459-19466.
53. A. Pandikumar, S. Murugesan and R. Ramaraj, *ACS Appl. Mater. Interfaces*, 2010, **2**, 1912-1917.
54 H. Yuan, D. Guo, X. Qiu, W. Zhu and L. Chen, *J. Power Sources*, 2009, **188**, 8-13.
55. Y. Bai, J. Wu, J. Xi, J. Wang, W. Zhu, L. Chen and X. Qiu, *Electrochem. Commun.*, 2005, **7**, 1087-1090

56. Y. Huang, H. Huang, Q. Gao, C. Gan, Y. Liu and Y. Fang, Electrochimica Acta, 2014, **149**, 34–41.

57. W. Zhuang, L. He, J. Zhu, R. An, X. Wu, L. Mu, X. Lu, L. Lu, X. Liu and H. Ying, Int. J. Hydrogen Energy, 2015, 403679-3688.

58. M. M. Shahid, A. Pandikumar, A. M. Golsheikh, N. M. Huang and H. N. Lim, *RSC Adv.*, 2014, **4**, 62793-62801.

59 R. Liang, A. Hu, J. Persic and Y. N. Zhou, Nano-Micro Lett. 2013, **5**, 202-212.

Table 1. Crystal data and refinement parameters for $[Cu_4Zr_6(\mu\text{-}O)_8(dmap)_4(OAc)_{12}]\bullet H_2O$ (**1**)

Empirical formula	$C_{44}H_{86}Cu_4N_4O_{37}Zr_6$
Formula weight	2064.64
Crystal system, Space group	Triclinic, *P* -1
a	12.0851(2) Å
b	13.2867(3) Å
c	23.8841(4) Å
α	77.8260(10)°
β	79.3910(10)°
γ	70.9570(10)°
Volume	3516.00(12) $Å^3$
Z	2
Calculated density	1.950 Mg/m^3
Absorption coefficient	2.126 mm^{-1}
F(000)	2060
Crystal size	0.360 x 0.210 x 0.150 mm^3

Crystal color and habit	Green Block
θ range for data collection	1.643 to 29.130°
Reflections collected	37836
Independent reflections	18727 (R_{int} = 0.0347)
Observed reflections [$I > 2\sigma(I)$]	13809
Completeness to θ = 25.242°	99.5 %
Data / restraints / parameters	18727 / 23 / 892
Goodness-of-fit on F^2	1.032
Final R indices [$I > 2\sigma(I)$]	R_1 = 0.0390, wR_2 = 0.0820
R indices (all data)	R_1 = 0.0613, wR_2 = 0.0913
Largest diff. peak and hole	0.962 and -0.879 (e Å^{-3})

Table 2. Coordination bond lengths for the structure $[Cu_4Zr_6(\mu\text{-}O)_8(dmap)_4(OAc)_{12}]\bullet H_2O$ (**1**)

Zr(1)-O(4)	2.073(2)	Zr(5)-O(27)	2.133(2)
Zr(1)-O(2)	2.077(2)	Zr(5)-O(28)	2.153(2)
Zr(1)-O(3)	2.191(2)	Zr(5)-O(30)	2.175(3)
Zr(1)-O(1)	2.203(2)	Zr(5)-O(5)	2.190(2)
Zr(1)-O(9)	2.259(2)	Zr(5)-O(3)	2.201(2)
Zr(1)-O(12)	2.265(2)	Zr(6)-O(4)	2.053(2)
Zr(1)-O(10)	2.302(2)	Zr(6)-O(8)	2.079(2)
Zr(1)-O(11)	2.336(2)	Zr(6)-O(32)	2.098(2)
Zr(2)-O(6)	2.055(2)	Zr(6)-O(7)	2.159(2)
Zr(2)-O(4)	2.083(2)	Zr(6)-O(33)	2.191(2)
Zr(2)-O(13)	2.107(2)	Zr(6)-O(3)	2.193(2)
Zr(2)-O(16)	2.144(3)	Zr(6)-O(35)	2.197(3)
Zr(2)-O(1)	2.182(2)	Cu(1)-O(13)	1.949(2)
Zr(2)-O(14)	2.191(2)	Cu(1)-O(7)	1.949(2)
Zr(2)-O(7)	2.208(2)	Cu(1)-O(34)	1.954(3)
Zr(3)-O(2)	2.056(2)	Cu(1)-N(1)	2.036(3)
Zr(3)-O(6)	2.079(2)	Cu(1)-O(35)	2.465(3)
Zr(3)-O(18)	2.109(2)	Cu(2)-O(15)	1.954(2)

Zr(3)-O(5)	2.189(2)	Cu(2)-O(1)	1.956(2)
Zr(3)-O(1)	2.191(2)	Cu(2)-O(18)	1.970(2)
Zr(3)-O(21)	2.191(2)	Cu(2)-N(2)	2.052(3)
Zr(3)-O(19)	2.199(2)	Cu(2)-O(17)	2.349(3)
Zr(4)-O(8)	2.074(2)	Cu(3)-O(27)	1.947(2)
Zr(4)-O(6)	2.080(2)	Cu(3)-O(20)	1.949(3)
Zr(4)-O(7)	2.166(2)	Cu(3)-O(5)	1.952(2)
Zr(4)-O(5)	2.182(2)	Cu(3)-N(3)	2.022(3)
Zr(4)-O(23)	2.256(2)	Cu(3)-O(21)	2.448(2)
Zr(4)-O(26)	2.258(2)	Cu(4)-O(31)	1.947(3)
Zr(4)-O(25)	2.325(3)	Cu(4)-O(3)	1.951(2)
Zr(4)-O(24)	2.340(3)	Cu(4)-O(32)	1.975(3)
Zr(5)-O(8)	2.065(2)	Cu(4)-N(4)	2.055(3)
Zr(5)-O(2)	2.088(2)	Cu(4)-O(29)	2.269(3)

Table 3. Comparison of electrocatalytic performance of some reported catalysts towards methanol oxidation

Catalysts	**Preparation method**	**Electrolyte**	**Medium**	**Scan Rate (mV/S)**	**Peak Potential (mV)**		**Current**	**Ref.**
					Forward Scan	**Reverse Scan**		
$Pt/CeO_2/CNTs$	two steps procedure Sol-gel and adsorption	0.5M H_2SO_4	Acidic	50	660	370	0.87 mA cm^{-2}	54
$Pt/TiO_2/CNTs$	two steps synthesis Sol-gel and adsorption	0.5M H_2SO_4	Acidic	50	680	390	0.55 mA cm^{-2}	
$Pt/SnO_2/CNTs$	two steps synthesis Sol-gel and adsorption	0.5M H_2SO_4	Acidic	50	670	420	o.43 mA cm^{-2}	
$Pt–ZrO_2/C$	two-step chemical reduction	0.1 M KOH	Alkaline	50	-270	400	25 mA cm^{-2}	55
$Pt/MnO_2/rGO$	Spontaneous and electroless method	0.5M H_2SO_4	Acidic	50	700	500	425 mA mg^{-1}	56
Pt/h-rGO@TiO_2-rGO	Deposition and hydrothermal method	0.5M H_2SO_4	Acidic	50	700	500	324 mA mg^{-1}	57

RGO–Co_3O_4	Hydrothermal method	0.1 M KOH	Alkaline	50	-150	-225	362 $\mu A\ cm^{-2}$	58
Pd/TiO_2-C	Hydrothermal growth method	0.1 M KOH	Alkaline	50	-200	-400	4 $mA\ cm^{-2}$	59
CuO-1.5ZrO_2	AACVD	0.1 M KOH	Alkaline	50	-250	-350	14 µA	Present work

Graphical Abstract

$CuO\text{-}1.5ZrO_2$ composite electrodes fabricated from a single source precursor $[Cu_4Zr_6(\mu\text{-}O)_8(dmap)_4(OAc)_{12}]\bullet H_2O$ have been utilized for the oxidation of methanol.